Fatty acid chain length drives lysophosphatidylserine-dependent immunological outputs

Neha Khandelwal[1,5], Minhaj Shaikh[2,5], Amol Mhetre[1,5],*, Shubham Singh[1,5], Theja Sajeevan[1], Alaumy Joshi[1,4], Kithiganahalli Narayanswamy Balaji[3], Harinath Chakrapani[2,*], Siddhesh S. Kamat[1,6,*].

[1]Department of Biology, Indian Institute of Science Education and Research (IISER) Pune, Dr. Homi Bhabha Road, Pashan, Pune 411008, Maharashtra, India.

[2]Department of Chemistry, Indian Institute of Science Education and Research (IISER) Pune, Dr. Homi Bhabha Road, Pashan, Pune 411008, Maharashtra, India.

[3]Department of Microbiology and Cell Biology, Indian Institute of Science (IISc), Bangalore 560012, Karnataka, India.

[4]Present address: Department of Biochemistry & Biophysics, Texas A&M University, College Station, Texas 77843, USA.

[5]These authors contributed equally to this work.

[6]Lead contact

*Correspondence to: siddhesh@iiserpune.ac.in; harinath@iiserpune.ac.in; amol@iiserpune.ac.in

SUMMARY/ABSTRACT:

Lysophosphatidylserines (Lyso-PSs) are potent lipid regulators of important immunological processes. Given their structural diversity and commercial paucity, here, we report the synthesis of a library of methyl-esters of lyso-PS, containing medium to very-long chain (VLC) lipid tails. We assay these lipids against ABHD12, deleterious mutations of which cause a human neurological disorder, and confirm this enzyme's preference for VLC lyso-PSs. Next, we demonstrate that VLC lyso-PSs orchestrate pro-inflammatory responses via a Toll-like receptor 2 dependent pathway, while long chain (LC) lyso-PSs signal through a putative G-Protein Coupled Receptor to influence macrophage activation. We also report that LC lyso-PSs best induce histamine release during mast cell degranulation, and that ABHD12 is a major lyso-PS lipase in these immune cells. Our findings thus illuminate a physiological balance between LC and VLC lyso-PSs, intricately regulated by ABHD12, and disrupting this fine-tuned homeostasis results in immunological outputs, that have detrimental pathological consequences in humans.

KEYWORDS:

INTRODUCTION

Lipids have long been known as potent signaling molecules that mediate many important physiological processes in mammals, including humans (Wymann and Schneiter, 2008, Dennis, 2016, Fahy et al., 2005). Prominent amongst these signaling lipids are the prostaglandins (Dennis and Norris, 2015), endocannabinoids (2-arachidonoylglycerol (2-AG) and anandamide (AEA)) (Blankman and Cravatt, 2013, Fowler et al., 2005), and the well-studied lysophospholipids (sphingosine 1-phosphate (S1P) (Gonzalez-Cabrera et al., 2014, Rosen et al., 2013) and lysophosphatidic acid (lyso-PA) (Ishii et al., 2004, Contos et al., 2000)). Given their physiological importance, the biosynthetic or metabolic enzyme(s) and/or cognate receptor(s) of the aforementioned lipids are either targets for drugs already in clinical use or under investigations in different phases of clinical trials for an array of human neurological and immunological disorders. Recently, the lysophosphatidylserines (lyso-PSs) have emerged as yet another important class of signaling lysophospholipids (Shanbhag et al., 2020), with potent bioactivities in the mammalian central nervous and immune system.

Cellular pharmacological studies have shown that lyso-PSs regulate several immunological processes (Shanbhag et al., 2020) like macrophage activation to clear apoptotic cells (Frasch and Bratton, 2012), mast cell degranulation (Lloret and Moreno, 1995), leukemic cell stimulation (Park et al., 2005), chemotaxis of human gliomas (Lee et al., 2008), and maturation of regulatory T-cells (Barnes et al., 2015), and perhaps signal through Toll-like receptors (van der Kleij et al., 2002) and/or G-Protein coupled receptors (GPCRs) (Inoue et al., 2012) in the mammalian nervous and immune system. Interestingly, and of biomedical relevance, mutations to putative lyso-PS receptors have been linked to different autoimmune diseases (Szymanski et al., 2014, Napier et al., 2015, Napier et al., 2014, Chu et al., 2013). Recent murine studies have shown that accumulation of lyso-PS, especially very long chain (VLC) lyso-PSs (Blankman et al., 2013), in the mammalian brain, is a major cause that drives the pathology of the early onset human neurological disorder PHARC (*p*olyneuropathy, *h*earing loss, *a*taxia, *r*etinitis pigmentosa, and *c*ataract) (Fiskerstrand et al., 2010, Fiskerstrand et al., 2009). Interestingly, PHARC is caused by deleterious mutations to

the *abhd12* gene (Fiskerstrand et al., 2010, Fiskerstrand et al., 2009), that encodes an integral membrane enzyme ABHD12 (α/β **h**ydrolase **d**omain containing protein # 12), a major, and to date, only *in vivo* functionally characterized lyso-PS lipase (Kamat et al., 2015, Blankman et al., 2013, Kelkar et al., 2019).

Given the strong link between lyso-PSs and human (patho)physiology, mechanistic studies are much needed to understand in more detail and biochemically characterize the signaling pathways influenced by lyso-PSs *in vivo*. The two factors complicating and/or limiting such studies are: (i) Unlike other signaling lipids (e.g. S1P, 2-AG, AEA), *in vivo* lyso-PSs are found with different fatty acids (ranging from medium to VLC) (Blankman et al., 2013, Barnes et al., 2015), and hence, the precise physiological contributions of the individual lyso-PSs remain cryptic; (ii) Commercially, lyso-PSs are limited, and even those available, are esterified only with long chain (LC) fatty acids (**Figure 1A**). Therefore, delineating the biological contributions of medium or VLC lyso-PSs has not been possible to date.

To address these problems, in this paper, we describe the synthesis of methyl-esters of lyso-PS (Me-lyso-PS) bearing saturated fatty acids of varying chain lengths ranging from C10 (medium) to C24 (VLC) having (*R*) or (*S*) configuration at the glycerol backbone. Next, we assay these Me-lyso-PS lipids against ABHD12 (Joshi et al., 2018, Kamat et al., 2015, Blankman et al., 2013), confirm this enzyme's preference for VLC lyso-PS lipids for the natural (*R*)-enantiomer, show its inability to turn over the unnatural (*S*)-enantiomer, and for first time report, that the ABHD12 catalyzed lyso-PS lipase reaction is highly stereoselective. Further, we test these Me-lyso-PS lipids in different immunological assays, and confirm that the naturally occurring (*R*)-enantiomer is significantly more biologically active than the corresponding (*S*)-enantiomer in all these assays performed by us in this study. Finally, we are the first to report, the contribution of individual lyso-PS lipids in macrophage activation and mast cell degranulation, show how the fatty acid chain length of lyso-PSs has a critical role to play in the output of these important immunological processes.

RESULTS.

Synthesis of Me-lyso-PS.

Structurally, lyso-PSs are composed of three building blocks: (i) a sugar backbone (glycerol), (ii) an amino acid head group (phospho-*L*-serine), and (iii) a lipid tail (fatty acid) (**Figure 1A**) (Fahy et al., 2011). It is this intricate combination of hydrophilic (glycerol and phospho-*L*-serine) and hydrophobic (fatty acid) biological building blocks that confers amphiphilic properties to lyso-PSs, that enables them to access different cellular membranes, organelles and compartments, and hence they serve as potent hormone-like mediators of different biological (immunological) processes (Vance, 2015, Tracey et al., 2018). From a stereochemical perspective, all natural lyso-PSs have two chiral centres: (i) α-carbon of the phospho-*L*-serine head group, and (ii) *sn-2* carbon of the (*R*)-glycerol backbone (**Figure 1A**) (Mallik et al., 2018). Biosynthetically, lyso-PSs are made from phosphatidylserine (PS) precursors, by the enzymatic action of PS-specific phospholipases (Hosono et al., 2001, Kamat et al., 2015), and subsequent studies have shown that physiologically almost all lyso-PSs exists as 1-(fatty acyl)-2-hydroxy-*sn*-glycero-3-phospho-*L*-serine (Iwashita et al., 2009b, Kamat et al., 2015). Given the synthetic challenges in making this bioactive lipid, only three naturally occurring LC lyso-PSs (**1a-c**) commercially available, thus limiting any rigorous structure activity relationship studies for this lipid class (**Figure 1A**). Since the commercial paucity of lyso-PSs would impede our proposed studies, here, we describe a facile synthesis route towards making Me-lyso-PS esterified with saturated fatty acids of varying chain lengths ranging from medium to VLC (**Figure 1B, S1, Supplementary Information**). Speculating that the free reactive carboxylate of the amino-acid might cross react and complicate the synthesis, we made Me-lyso-PSs, which show almost identical bioactivities to canonical natural lyso-PSs in some previously reported biological assays (Ikubo et al., 2015). Our synthetic route, successfully afforded the naturally occurring (*R*)-Me-lyso-PSs (**Figure S1**) and the unnatural (*S*)-Me-lyso-PSs (**Figure S2**) with same fatty acids (**Figure 1B**), to yield final compounds ((*R*)-**2a-h** or (*S*)-**2a-h**) in milligram quantities.

ABHD12 prefers VLC lyso-PSs as substrates.

Having synthesized a (*R*)- and (*S*)-Me-lyso-PS library, we first tested whether these lipids were indeed substrates for the mammalian lyso-PS lipase ABHD12. Leveraging established liquid-chromatography coupled to mass spectrometry (LC-MS) based substrate assays (Joshi et al., 2018), we found that both recombinant human ABHD12 (hABHD12) and endogenous mouse brain ABHD12 (mABHD12) robustly turned over (*R*)-Me-lyso-PSs, and for the same fatty acid, (*R*)-Me-lyso-PS and corresponding canonical natural lyso-PS behaved almost identically (**Figure S3, Table 1**). Next, we performed enzyme kinetics measurements for our (*R*)-Me-lyso-PS library against hABHD12, and found that, hABHD12 strongly prefers VLC (*R*)-Me-lyso-PSs as substrates (**Figure 2A, Table 1**). Further, mouse brain membrane lysates were assayed against this library, and we found that mABHD12 also prefers VLC (*R*)-Me-lyso-PSs (**Figure 2B**). In this experiment, mouse brain membrane lysates from ABHD12 knockout mice were used as controls, to delineate specific contributions from mABHD12 (**Figure 2B**). In both assays, we also tested (*S*)-Me-lyso-PSs, and found that, these were in fact very poor substrates for hABHD12 and mABHD12 (**Figure S3**), with catalytic efficiencies 100-fold lower than that of corresponding (*R*)-Me-lyso-PSs for hABHD12 (**Table 1**). Taken together, the substrate assays conclusively show for the first time, that the ABHD12 catalyzed lyso-PS lipase reaction is highly stereospecific, prefers VLC (*R*)-lyso-PSs as substrates, and, together with recent findings, now provides a solid biochemical explanation as to why VLC lyso-PSs accumulate most in ABHD12 knockout mouse brains (Blankman et al., 2013).

VLC lyso-PSs signal via TLR2 in mammalian macrophages.

Lyso-PSs elicit pro-inflammatory responses via cytokine secretion (e.g. TNF-α, IL-6) from mammalian macrophages (Kamat et al., 2015, Frasch and Bratton, 2012) and we first assessed if Me-lyso-PSs were capable of the same. When primary peritoneal macrophages (PPM) isolated from wild type (WT) or ABHD12 knockout were incubated with Me-lyso-PSs,

we found that VLC (*R*)-Me-lyso-PSs, (*R*)-**2g** and (*R*)-**2h**, produced the highest pro-inflammatory cytokine secretion (TNF-α, IL-6) from WT PPM (**Figures 3A, S4, S5**). Not surprisingly, ABHD12-null PPM secreted significantly more pro-inflammatory cytokines (TNF-α, IL-6) compared to WT PPM, consistent with their diminished lyso-PS lipase activity(Kamat et al., 2015) (**Figures 2A, S5**). Interestingly, treating PPM with unnatural (*S*)-Me-lyso-PSs failed to elicit any inflammatory response (**Figures S4, S5**), suggesting that lyso-PS recognition in PPM is highly stereospecific. Reported literature speculates that VLC lyso-PSs signal through TLR2 (van der Kleij et al., 2002), and large-scale gene expression databases (Wu et al., 2016) show that TLR2, but no other putative lyso-PS receptors, is enriched on PPM (**Figure S6**). We found that pharmacological antagonism of TLR2 using Sparstolonin B (SpaB) (a dual TLR2/TLR4 antagonist) (Liang et al., 2011), ablated the increased pro-inflammatory cytokine secretion (TNF-α, IL-6) caused by VLC (*R*)-Me-lyso-PSs in WT PPM (**Figure 3B, S5**). We found that human THP-1 macrophages also showed similar results (**Figure S7**).

Next, we harvested PPM from TLR2 knockout mice (Holla et al., 2016), and measured pro-inflammatory cytokine secretion (TNF-α, IL-6), following (*R*)-Me-lyso-PS treatment. Consistent with pharmacological studies, we found that VLC (*R*)-Me-lyso-PSs, (*R*)-**2g** and (*R*)-**2h,** produced highest pro-inflammatory cytokine secretion (TNF-α, IL-6) from WT PPM, and this secretion was almost absent in TLR2-null PPM (**Figures 3C**, **S8**). ABHD12 knockout mice display increased cerebellar microgliosis, where accumulation of VLC lyso-PSs speculatively causes this neuroinflammatory phenotype (Blankman et al., 2013). To test if VLC lyso-PSs indeed causes neuroinflammation, and if in fact, they signal through TLR2, we intravenously injected a VLC (*R*)-Me-lyso-PS ((*R*)-**2h**) into WT or TLR2-null mice, and quantified neuroinflammation by the number of activated microglia using established immunohistochemical analysis (Singh et al., 2020, Blankman et al., 2013). We find that systemic administration of (*R*)-**2h** robustly induced cerebellar microgliosis in WT, but not TLR2 knockout mice, suggesting that VLC (*R*)-Me-lyso-PSs indeed signal through

TLR2, causing neuroinflammation (**Figures 3D**, **S9**). Interestingly, a LC (*R*)-Me-lyso-PS ((*R*)-**2e**) did not produce any neuroinflammation in WT mice (**Figure S9**). Taken together our results provide compelling *in vivo* evidence that, VLC lyso-PSs signal through TLR2, elicit a robust pro-inflammatory immune response and are likely responsible for the neuroinflammation observed in ABHD12 knockout mice, the murine model of PHARC.

Mammalian macrophages have a cryptic lyso-PS receptor.

Macrophages in response to lyso-PS display increased intracellular cyclic adenosine 5'-monophosphate (cAMP) (Sugita et al., 2013), cytosolic calcium (Ca^{2+}) flux (Park et al., 2005) and heightened phosphorylation of the nodal e̲xtracellular signal-r̲egulated k̲inase (ERK) (Lee et al., 2008, Sugita et al., 2013), and we wanted to test if Me-lyso-PSs also produces these phenotypes. We found in PPM that cellular cAMP (**Figure 4A**), cytosolic Ca^{2+} levels (**Figure 4B**), and ERK phosphorylation (**Figure 4C**) increased most profoundly upon treatment with LC (*R*)-Me-lyso-PSs, especially (*R*)-**2e**, and, medium or VLC (*R*)-Me-lyso-PS had negligible effect on these phenotypes. Also, unnatural (*S*)-Me-lyso-PSs failed to elicit any response for any of these phenotypes (**Figure S10**). Surprisingly, genetic deletion or pharmacological antagonism of TLR2 showed no effect on any of these phenotypes in PPM or human THP-1 macrophages (**Figures S11-14**). Of note, brains and lipopolysaccharide (LPS) treated PPM derived from ABHD12-null mice, (where, in concentration, **1b** is the most abundant, and significantly deregulated lyso-PS (Blankman et al., 2013, Kamat et al., 2015)), have markedly more phosphorylated ERK compared to a WT control (**Figure 4D**). Given the heightened intracellular cAMP, cytosolic Ca^{2+} influx, ERK phosphorylation, and inability of pharmacological antagonism or genetic disruption of TLR2 to affect these phenotypes, strongly supports the existence of another lyso-PS receptor on mammalian macrophages in addition to TLR2 (**Figure 4E**). We speculate, based on aforementioned phenotypes, that the as-of-yet unknown receptor, is likely an unannotated GPCR (as putative lyso-PS GPCRs (Inoue et al., 2012) are absent in macrophages (**Figure**

S6)) that prefers LC lyso-PSs as ligands, to produce its downstream biological effects (**Figure 4E**).

LC lyso-PSs robustly induce mast cell degranulation.

Histamine release from mast cell degranulation is perhaps, the most investigated lyso-PS mediated immunological response (Sugo et al., 2006, Iwashita et al., 2009a), and yet contribution of individual lyso-PSs to this phenotype and process remain poorly understood. To address this, we generated peritoneal-derived cultured mast cells (PCMCs) (Meurer et al., 2016), and confirmed their ability to degranulate in presence of **1a** or the corresponding (*R*)-Me-lyso-PS, (*R*)-**2d** (**Figure 5A**) (Iwashita et al., 2009a, Sugo et al., 2006). We quantitatively measured histamine release using an established LC-MS assay (Chimalakonda et al., 2015) (**Figure S15**), and found that **1a** and (*R*)-**2d** had comparable half-maximal effective concentration (EC_{50}) towards inducing PCMC degranulation, while the unnatural (*S*)-**2d** failed to induce PCMC degranulation (**Figure 5B**), suggesting that the putative receptor on PCMCs (likely GPR34 (Iwashita et al., 2009b, Sugo et al., 2006), **Figure S6**) is stereoselective in lyso-PS (ligand) recognition. Next, we performed exhaustive dose response studies with (*R*)-Me-lyso-PSs and found that (*R*)-**2d** most potently induced degranulation, with other LC (*R*)-Me-lyso-PSs (*R*)-**2e** and (*R*)-**2c** following suite (**Figure 5C**). The (*R*)-Me-lyso-PSs containing medium chain (< C12) or VLC ($\geq$ C20) lipids failed to induce PCMC degranulation (**Figure 5C**), suggesting that besides the head group, the lipid chain length recognition is major factor contributing to this phenotype.

ABHD12 is a major lyso-PS lipase in primary mast cells.

ABHD12 is a major lyso-PS lipase in different immune cells (Ogasawara et al., 2018, Kamat et al., 2015), but its function in mast cells remains unknown. Western blot analysis (**Figure 6A**) and diminished lyso-PS lipase activity (**Figure 6B**) confirmed the loss of ABHD12 in PCMCs derived from ABHD12-null mice, and ABHD12-null PCMCs secreted significantly more lyso-PS (~ 2-fold more **1a** and **1b**) compared to WT PCMCs (**Figure 6C**).

Given the diminished lyso-PS lipase activity, we postulated that **1a** treatment would cause ABHD12-null PCMCs to degranulate more efficiently than WT PCMCs. Indeed, ABHD12-null PCMCs released histamine more effectively than WT PCMCs upon **1a** treatment (**Figure 6D**). Finally, we measured serum histamine concentrations following intravenous (*R*)-**2d** injection in WT or ABHD12 knockout mice, and found that ABHD12-null mice displayed heightened circulating histamine concentrations compared to WT mice (**Figure 6E**). These results together confirm ABHD12's role as a major lyso-PS lipase in mast cells, where by regulating serum lyso-PS concentrations (**Figure 6E**), it controls systemic histamine release.

DISCUSSION.

Signaling lipids are potent hormone-like biological molecules which regulate several important physiological processes in mammals and their deregulation often has detrimental consequences that eventually manifests into disease in humans. Given their direct link to human diseases (Napier et al., 2015, Szymanski et al., 2014, Napier et al., 2014, Chu et al., 2013, Fiskerstrand et al., 2010, Fiskerstrand et al., 2009, Blankman et al., 2013), the lyso-PSs have been the focus of several recent studies (Ogasawara et al., 2018, Kamat et al., 2015, Blankman et al., 2013, Barnes et al., 2015, Inoue et al., 2012, Iwashita et al., 2009b), which have greatly expanded the physiological repertoire of the signaling lipids (Shanbhag et al., 2020). However, unlike the more established signaling lipids (e.g. 2-AG, AEA, S1P, lyso-PA), *in vivo* lyso-PSs exist esterified with different fatty acids ranging from medium to VLC (C10-C24) (Kamat et al., 2015, Blankman et al., 2013, Barnes et al., 2015). Given the vast diversity in their *in vivo* content, it remains unclear as to which of these lyso-PSs have signaling functions or capabilities, and how they influence different immunological processes. The lack of detailed structure activity relationship studies for these immunological phenotypes for lyso-PSs stems largely from the limited commercially availability, and reported synthetic strategies towards making them.

In this paper, we synthesize a Me-lyso-PS library bearing (*R*)- or (*S*)-stereochemistry at the sn-2 glycerol position (**Figure 1, Supplementary Information**). We find that (*R*)-Me-

lyso-PSs serve as excellent and bioequivalent surrogates for natural lyso-PSs in all biological assays, while (*S*)-Me-lyso-PSs are biologically inactive. Using this Me-lyso-PS library, by substrate profiling assays, we show conclusively that the lyso-PS lipase ABHD12 is highly stereoselective, and prefers VLC lysos-PSs are substrates (**Figure 2**). We also report the distinct role that the fatty acid chain length of individual lyso-PSs plays in the activation of macrophages (**Figures 3, 4**) and mast cell degranulation (**Figures 5, 6**). That VLC lyso-PSs signal through TLR2 and causes neuroinflammation (**Figure 3**) raises an intriguing possibility that the neurological disease PHARC may itself be an autoimmune disease.

Projecting ahead, we propose that the functional antagonism of TLR2 might provide an excellent therapeutic paradigm in treating PHARC. This premise can be tested genetically by generating and characterizing ABHD12-TLR2 dual knockout mice, and pharmacologically by discovering much needed *in vivo* active TLR2 functional antagonists. Next, the annotation of ABHD12 as a major lyso-PS lipase in primary mast cells provides yet another avenue in understanding the immunomodulatory properties and the functional cross-talk of lyso-PS lipids between different immune cells particularly in the context of allergies and autoimmune conditions (Kelkar et al., 2019, Ogasawara et al., 2018). Finally, we would like to note that a major shortcoming of our study, is the inability of our synthetic strategy in making Me-lyso-PSs bearing unsaturated fatty acid chains. Therefore, the development of such a synthetic methodology, would not only enable making Me-lyso-PSs bearing unsaturated fatty acid chains, but can also be leveraged to generate lyso-PS probes with suitable biorthogonal handles (e.g. photoreactive groups like diazarine or enrichment handles like an alkyne). Such lyso-PS probes in tandem with advanced LC-MS based chemoproteomics platforms will greatly facilitate the identification of hitherto unknown protein ligands and/or receptors of lyso-PSs, and this new knowledge will certainly expand our biological understanding for this emerging immunomodulatory lipid class.

Author contributions: N.K., S.S., T.S., and A.J. performed all the biochemical studies described in this paper. M.S. and A. M. synthesized and characterized all the compounds described in this paper; A.M. and H.C. supervised the synthesis. K.N.B. provided the TLR2 knockout mice for this study. S.S.K. conceived the project, acquired funding and wrote the paper with inputs from all authors.

Competing interests: The authors declare no competing financial interests.

Data and materials availability: The authors declare that all the data that supports the findings of this study are available in the paper, and the associated supplementary information. Any further information or data or any chemical compounds can be made available by the lead contact upon reasonable request.

Additional Information

Supplementary information is available with the online version of this paper.

- Supplementary Figures 1 – 15

- Chemical synthesis and compound characterization

- Spectral data of synthesized compounds

METHODS.

Materials. Unless otherwise mentioned, all the following materials used in the experiments described in this paper were purchased from the source mentioned in the parenthesis: chemicals, buffers and reagents (Sigma-Aldrich), commercial lipids and lipid standards (Avanti Polar Lipids), primary and secondary antibodies (Abcam), and tissue culture media and Fetal Bovine Serum (FBS) (HiMedia).

Mouse studies. All animal (mouse) studies and experiments described in this paper have received formal approval from the Indian Institute of Science Education and Research, Pune – Institutional Animal Ethics Committee (IISER-P IAEC) (application no: IISER_Pune IAEC/2019_2/07) constituted as per the guidelines and norms provided by the Committee for the Purpose of Control and Supervision of Experiments in Animals (CPCSEA), Government of India. Thioglycollate elicited primary peritoneal macrophages (PPMs) (Kamat et al., 2015) and peritoneal-derived cultured mast cells (PCMCs) (Meurer et al., 2016) were generated and harvested from mice and cultured using established protocols. Their pharmacological treatments are described in the subsequent sections.

Lyso-PS lipase substrate assays. Wild type (WT) human ABHD12 (hABHD12) or the catalytically inactive active site mutant S246A hABHD12 were transiently transfected in HEK293T cells along with mock transfection controls, and the membrane lysates from these were prepared as reported earlier (Kelkar et al., 2019, Joshi et al., 2018). The brain membrane lysates from wild type and ABHD12 knockout mice were also prepared using a protocol reported earlier (Joshi et al., 2018, Singh et al., 2020). The lyso-PS lipase assays described in this paper were performed using an established LC-MS method that measures the free fatty released from lyso-PS substrates by the lipase activity of ABHD12 (Joshi et al., 2018, Singh et al., 2020). All assays done using 10 μg of HEK293T membrane lysates transfected with hABHD12 or 20 μg of brain membrane lysates for 30 mins, as previous

studies have shown that the lyso-PS lipase assay is linear for this protein concentration and time over a range of substrate concentrations (Joshi et al., 2018). All single concentration lipase (substrate) assays were done using 100 μM of the lipid substrate, while the enzyme kinetic studies were done over the concentration range of 0 – 400 μM for the particular lipid that was assayed.

Mammalian cell culture and lipid treatments. All cultured mammalian cell lines (HEK293T and THP-1) were purchased from the ATCC, and cultured in RPMI1640 medium supplemented with 10% (v/v) FBS and antibiotics (1% (v/v) penicillin-streptomycin (MP Biomedicals)) at 37 °C with 5% (v/v) CO_2. Cell staining with 4',6-diamidino-2-phenylindole (DAPI) was routinely performed to ensure that all cell lines were devoid of any mycoplasma contamination. All live cells were estimated on a TC20 automated cell counter using trypan blue reagent as per manufacturer's protocol (Bio-Rad). For the pro-inflammatory cytokine measurements, macrophages (1 x 10^6 PPMs or 0.5 x 10^6 THP-1 cells) were plated in 6-well plates (Eppendorf) in 2 mL of RPMI1640 media without any supplementation, and treated with vehicle (DMSO) or lipids [commercial lyso-PSs **1a**, **1b**, or (*R*)-Me-lyso-PSs ((*R*)-**2a-h**) or (*S*)-Me-lyso-PSs ((*S*)-**2a-h**) or free fatty acids] or other assay controls (LPS or glycerophosphoserine (GPS) head group) all at 1 μM final concentration for 4 h at 37 °C. Following this treatment, the media (1.5 mL) was collected and stored at – 80 °C till the analysis was completed. The pro-inflammatory cytokines (TNF-α and IL-6) were quantitatively measured using standard single analyte ELISA assays as per manufacturer's instructions (R&D Systems). For the cellular cyclic adenosine 5'-monophosphate (cAMP), cytosolic calcium (Ca^{2+}) and phosphorylated ERK measurements, macrophages (4 x 10^6 PPMs or 2 x 10^6 THP-1 cells) were plated in 6-well plates (Eppendorf) in 3 mL of RPMI1640 media without any supplementation, and treated with vehicle (DMSO) or lipids [commercial lyso-PSs **1a**, **1b**, or (*R*)-Me-lyso-PSs ((*R*)-**2a-h**) or (*S*)-Me-lyso-PSs ((*S*)-**2a-h**) or free fatty acids] or other assay controls (LPS or GPS head group) all at 1 μM final concentration for 10

mins at 37 °C. Following this treatment, the assay plates were centrifuged at 1400g for 5 min to pellet the live cells, and separate the media. The media was removed by pipetting, following which, the cells were washed with sterile cold Dulbecco's phosphate buffer saline (DPBS) (x 3 times) at 4 °C, and lysed by sonication in 500 μL cold sterile DPBS at 4 °C. The cell lysates were deproteinized by passing them through a 3000 (3-kDa) molecular weight filter, and the flow through was eventually used to estimate the cellular levels of cAMP, free cytosolic Ca^{2+} and phosphorylated ERK. The changes (increase) in cellular cAMP, free cytosolic Ca^{2+} and ERK phosphorylation in response to the aforementioned treatments were quantitatively estimated using standard competitive ELISA based colorimetric (cAMP, ERK phosphorylation) and fluorometric (free cytosolic Ca^{2+}) assays as per manufacturer's instructions (Abcam). All pharmacological TLR2 antagonism studies (Liang et al., 2011, Liang et al., 2013) described in this paper, were done at 10 μM final concentration of SpaB for 4 h at 37 °C.

Western blot analysis. Cell or tissue lysates were prepared as described earlier (Joshi et al., 2018), and the protein concentrations were estimated using the Pierce BCA Protein Assay kit (Thermo Fisher Scientific). Thereafter, 50 μg protein lysate was resolved on a 12% SDS-PAGE gel and transferred onto a PVDF membrane (GE Healthcare) (60 mA, 12 h, 4 °C). Post-transfer, the membrane was blocked with 5% (w/v) skimmed milk in 1X phosphate buffered saline containing 0.1% (w/v) Tween-20 (PBST) (blocking buffer) for 1 h at room temperature (20 – 25 °C), washed with PBST (x 3 times) and subsequently probed with the primary antibody (dilution 1:1000 to 1:10000 depending on the antibody) in blocking buffer for 12 – 14 h at 4 °C. Following this, the membrane was washed with PBST (x 3 times), and incubated with a horse-radish peroxidase (HRP) conjugated anti-rabbit IgG (H + L) (goat, Thermo Fisher Scientific, 31460, 1:10,000) or HRP-conjugated anti-mouse IgG (H + L) (goat, Abcam, ab6789, 1:10,000) secondary antibody for 1 h at room temperature (20 – 25 °C). Finally, the membrane was washed with PBST (x 3 times), and the signal was visualized

with SuperSignal West Pico Chemiluminescent substrate (Thermo Fisher Scientific) on a Syngene G-Box Chemi-XRQ gel documentation system. For the phosphoprotein immunoblotting, the cells and tissues were lysed in buffer containing phosphatase inhibitors (1 mM sodium orthovanadate, 1 mM sodium pyrophosphate, 5 mM sodium fluoride) to maintain intact protein phosphorylations at serine, threonine and/or tyrosine protein residues. In this study, the following primary antibodies were used: anti-phospho-ERK (rabbit, Cell Signaling Technology, Cat: 20G11, dilution 1:1000), anti-total ERK (rabbit, Cell Signaling Technology, Cat: 137F5, dilution 1:1000), anti-ABHD12 (rabbit, Abcam, Cat: ab182011, dilution 1:2000), and anti-actin (rabbit, Cloud-Clone Corp, Cat: CAB340Hu01, dilution 1:1000).

ELISA kits. All quantitative pro-inflammatory cytokine measurements (TNF-α, IL-6) were done using single analyte ELISA assays from R&D Systems as per manufacturer's instructions. The following ELISA kits were used: mouse TNF-alpha DuoSet (Cat: DY410), mouse IL-6 DuoSet (Cat: DY406), human TNF-alpha DuoSet (Cat: DY210), and human IL-6 DuoSet (Cat: DY206). For measuring intracellular cAMP, cytosolic free Ca^{2+} and phosphorylated ERK, ELISA kits were purchased from Abcam, and the assays were performed as per manufacturer's instructions. The following kits were used for the same: cAMP assay kit (competitive ELISA) (Cat: ab65355); Fluo-8 calcium assay kit – medium removal (Cat: ab112128); and ERK1 (pT202/pY204) + ERK2 (pT185/pY187) + total ERK1/2 ELISA kit (Cat: ab126445).

RT-PCR. The total RNA was isolated from mouse PPM using the RiboZol^{TM} RNA extraction reagent (Amresco), and the first strand cDNA was synthesized from the isolated total RNA using the ThermoScript^{TM} RT-PCR System (Invitrogen) as per manufacturer's protocol. The primers listed below were used to yield the fragment size in parenthesis for the following gene products for the gel represented in **Figure S6**:

GRP34: 5'-GAGCACTTCGGCTTACTTGG-3' and 5'-TTCCATGAGAGGAGCAAAGC-3' (422-bp);

GPR174: 5'-CTGCATCAGTGTGCGAAGAT-3' and 5'-TCACTCTTCTGGCAAAGCAA-3' (479-bp);

P2Y10: 5'-AAGAGCCCAGCTGACACAAC-3' and 5'-AAGAGCCCAGCTGACACAAC-3' (439-bp);

TLR2: 5'-GACTCACAGCAGCCATGAAA-3' and 5'- TCGCGGATCGACTTTAGACT-3' (451-bp);

ACTB: 5'-GGGAATGGGTCAGAAGGACT-3' and 5'-ACGCTCGGTCAGGATCTTC-3' (454-bp);

GAPDH: 5'-ACTTGAAGGGTGGAGCCAAA-3' and 5'- AGATCCACGACGGACACATT-3' (403-bp).

Immunohistochemical analysis. The immunohistochemical analysis were done using a protocol recently published by us with minor modifications (Singh et al., 2020). Briefly, mice were deeply anaesthetized using isoflurane and perfused first with cold phosphate buffer saline (PBS), and then with 4% (w/v) paraformaldehyde (PFA) in PBS. Brains were dissected and post-fixed in 4% (w/v) PFA in PBS overnight at 4 °C and then transferred into 30% (w/v) sucrose in PBS until brains sank to bottom of the tubes (~ 3 days). Coronal 25 μm cerebellar sections were cut on a freezing microtome (Leica CM1950), maintained at – 30 °C and 1 out of every 6 sections was collected for assessing microglial activation. Endogenous peroxidases were inactivated with 3% (v/v) hydrogen peroxide in PBS for 15 min. Thereafter the sections were washed twice with 1% bovine serum albumin (BSA) (HiMedia) in PBS, and permeabilized with 0.1% (w/v) Triton-X 100 and 0.5% (w/v) BSA in PBS at room temperature (20 – 25 °C) for 45 mins. The sections were then incubated with primary monoclonal anti-Iba1 antibody [rabbit, Abcam, Cat: ab178846, 1:1000] in 1% (w/v) BSA in PBS overnight at 4 °C. Following overnight incubation, the sections were washed three

times with 0.5% (w/v) BSA in PBS and incubated with secondary antibody, biotinylated anti-rabbit [horse, Vector labs, BP-1100, 1:500] in 0.5% (w/v) BSA in PBS for 1 h at room temperature (20 – 25 °C). Following this treatment, the sections were washed twice in 0.5 % (w/v) BSA in PBS, incubated with ABC Elite Vectastatin (Vector labs, Cat: PK-6100) for 1 h at room temperature (20 – 25 °C) and subsequently washed twice with excess PBS. Finally, the sections were stained with Immpact DAB (Vector labs, Cat: SK-4105) for 3 min in the dark, transferred to excess PBS and mounted in VectaMount (Vector labs, Cat: H-5000) after drying. Activated microglial cells (area > 200 μm^2) in matching cerebellar sections were quantified using the ImageJ software (NIH) (Rueden et al., 2017) as per previously described protocols (Blankman et al., 2013, Singh et al., 2020).

Histamine estimation from mast cells. The PCMCs were isolated from the peritoneal cavity of C57Bl/6 mice and cultured using a previously reported protocol with typical yields of 1 million PCMCs per mouse (Meurer et al., 2016). To assess the extent of lyso-PS induced degranulation of PCMCs, histamine release from these cells was measured using an established LC-MS method (Chimalakonda et al., 2015). Towards this, PCMCs were first pelleted (1400g for 5 min) and subsequently re-suspended in Hank's Balanced Salt Solution (HBSS) containing 1% (w/v) heat inactivated FBS at a concentration of 5×10^6 cells/mL. All assays were performed in a 96 well plates with "V" bottoms (Tarsons) to a final volume of 100 μL at 37 °C with 5% (v/v) CO_2. The vehicle (DMSO) or lipids (commercial lyso-PSs or (R)-Me-lyso-PSs ((R)-**2a-h**) or (S)-Me-lyso-PSs ((S)-**2a-h**); ranging from 1 nM – 100 μM concentration in the assay) were added to individual wells with or without Concanavalin A (1 mg/mL final assay concentration) to make volume to 90 μL in HBSS. To this, 10 μL of the PCMC cell stock (5×10^6 cells/mL) pre-incubated at 37 °C with 5% (v/v) CO_2 was added such that each assay well finally contained 5×10^3 cells, and the assay allowed to proceed for 30 mins at 37 °C with 5% (v/v) CO_2. At this point, to quench the assay, the cells were pelleted by centrifugation (1200g for 5 mins), and 50 μL of the media was collected for

estimation of secreted histamine levels. To this 50 μL of media, 150 μL of LC-MS grade acetonitrile (Sigma-Aldrich) was added, the mixture was vortexed and stored at – 80 °C till the histamine estimations were performed by LC-MS. The pellet cells were re-suspended in the remaining 50 μL media by vigorous vortexing and lysed by sonication in a water bath at 37 °C. The cell lysates were then added to 150 μL of MS grade acetonitrile (Sigma-Aldrich), the mixture was vigorously vortexed and stored at – 80 °C till the histamine estimations were performed. The histamine release from PCMCs was calculated in accordance to the established formula for the LC-MS method (Chimalakonda et al., 2015). For measuring circulating serum histamine concentrations, 1 volume of mouse serum (200 – 300 μL) obtained from whole blood of wild type or ABHD12 knockout mice, was mixed with 2 volumes (400 – 600 μL) MS grade acetonitrile (Sigma-Aldrich), the mixture was centrifuged at 2000g for 5 mins to pellet the protein debris, and the supernatant was collected, dried, and re-suspended in 50 μL MS grade acetonitrile (Sigma-Aldrich), and assessed thereafter by LC-MS as per a previously reported protocol (Chimalakonda et al., 2015). The quantitation for serum histamine levels, was done using a standard calibration curve for histamine (5 – 5000 ng/mL serum). All histamine measurements were done using an established LC-MS/MS method (Chimalakonda et al., 2015) in the positive ion mode using high resolution multiple reaction monitoring (MRM-HR) analysis on a Sciex X500R quadrupole time-of flight (QTOF) mass spectrometer fitted with an Exion UHPLC system using a Kinetex 2.6 μm HILIC column with 100 Å particle size, 150 mm length and 3 mm internal diameter (Phenomenex). The MRM-HR mass spectrometry parameters for measuring histamine are: precursor ion mass (Q1, M+H$^+$) = 112.0869, product ion mass (Q3, M+H$^+$) = 95.0604, declustering potential = 100 V, entrance potential = 10 V, collision energy = 50 V, and collision exit potential = 10 V. Complete details of the sensitivity and dynamic range of the LC-MS method for histamine estimation, as well as co-elution studies with a histamine standard can be found in **Figure S15**.

Lyso-PS measurements. The organic extractions to enrich for lyso-PS lipids, and all the LC-MS based quantitative lyso-PS measurements (secreted lyso-PS concentrations from PCMCs (**Figure 6C**), and the serum lyso-PS levels (**Figure 6E**)) were performed using an established and previously reported protocol (Kelkar et al., 2019, Singh et al., 2020).

Synthesis and compound characterization. Complete details of the synthesis of the compounds reported in this paper and their chemical and analytical characterization can be found in the **Supplementary Information**.

Statistical analysis. All data represented in this paper is shown as mean $\pm$ standard deviation unless otherwise mentioned. All statistical analyses were performed using the GraphPad Prism 7 (version 7.0b) software for Mac OS X. The Student's two-tailed t test was used to determine the statistical significance between the different study group, and a P value of < 0.05 was considered statistical significant for this study.

References.

BARNES, M. J., LI, C. M., XU, Y., AN, J., HUANG, Y. & CYSTER, J. G. 2015. The lysophosphatidylserine receptor GPR174 constrains regulatory T cell development and function. *J Exp Med,* 212**,** 1011-20.

BLANKMAN, J. L. & CRAVATT, B. F. 2013. Chemical Probes of Endocannabinoid Metabolism. *Pharmacological Reviews,* 65**,** 849-871.

BLANKMAN, J. L., LONG, J. Z., TRAUGER, S. A., SIUZDAK, G. & CRAVATT, B. F. 2013. ABHD12 controls brain lysophosphatidylserine pathways that are deregulated in a murine model of the neurodegenrative disease PHARC. *Proc. Natl. Acad. Sci. U.S.A.,* 110**,** 1500-1505.

CHIMALAKONDA, K. C., PANG, E., WEAVER, J. L., HOWARD, K. E., PATEL, V. & BOYNE, M. T. 2015. Development and validation of a liquid-chromatography tandem mass spectrometry method to determine in vitro and in vivo histamine release. *Journal of Pharmaceutical and Biomedical Analysis,* 102**,** 494-499.

CHU, X., SHEN, M., XIE, F., MIAO, X. J., SHOU, W. H., LIU, L., YANG, P. P., BAI, Y. N., ZHANG, K. Y., YANG, L., HUA, Q., LIU, W. D., DONG, Y., WANG, H. F., SHI, J. X., WANG, Y., SONG, H. D., CHEN, S. J., CHEN, Z. & HUANG, W. 2013. An X chromosome-wide association analysis identifies variants in GPR174 as a risk factor for Graves' disease. *J Med Genet,* 50**,** 479-85.

CONTOS, J. J. A., ISHII, I. & CHUN, J. 2000. Lysophosphatidic acid receptors. *Mol Pharm,* 58**,** 1188-1196.

DENNIS, E. A. 2016. Lipidomics In Disease And Drug Discovery. *Faseb Journal,* 30.

DENNIS, E. A. & NORRIS, P. C. 2015. Eicosanoid storm in infection and inflammation. *Nature Reviews Immunology,* 15**,** 511-523.

FAHY, E., COTTER, D., SUD, M. & SUBRAMANIAM, S. 2011. Lipid classification, structures and tools. *Biochimica Et Biophysica Acta-Molecular and Cell Biology of Lipids,* 1811**,** 637-647.

FAHY, E., SUBRAMANIAM, S., BROWN, H. A., GLASS, C. K., MERRILL, A. H., JR., MURPHY, R. C., RAETZ, C. R., RUSSELL, D. W., SEYAMA, Y., SHAW, W., SHIMIZU, T., SPENER, F., VAN MEER, G., VANNIEUWENHZE, M. S., WHITE, S. H., WITZTUM, J. L. &

DENNIS, E. A. 2005. A comprehensive classification system for lipids. *J Lipid Res,* 46**,** 839-61.

FISKERSTRAND, T., H'MIDA-BEN BRAHIM, D., JOHANSSON, S., M'ZAHEM, A., HAUKANES, B. I., DROUOT, N., ZIMMERMANN, J., COLE, A. J., VEDELER, C., BREDRUP, C., ASSOUM, M., TAZIR, M., KLOCKGETHER, T., HAMRI, A., STEEN, V. M., BOMAN, H., BINDOFF, L. A., KOENIG, M. & KNAPPSKOG, P. M. 2010. Mutations in ABHD12 cause the neurodegenerative disease PHARC: An inborn error of endocannabinoid metabolism. *Am J Hum Genet.,* 87**,** 410-7.

FISKERSTRAND, T., KNAPPSKOG, P., MAJEWSKI, J., WANDERS, R. J., BOMAN, H. & BINDOFF, L. A. 2009. A novel Refsum-like disorder that maps to chromosome 20. *Neurology,* 72**,** 20-27.

FOWLER, C. J., HOLT, S., NILSSON, O., JONSSON, K. O., TIGER, G. & JACOBSSON, S. O. 2005. The endocannabinoid signaling system: pharmacological and therapeutic aspects. *Pharmacol Biochem Behav,* 81**,** 248-62.

FRASCH, S. C. & BRATTON, D. L. 2012. Emerging roles for lysophosphatidylserine in resolution of inflammation. *Prog Lipid Res.,* 51**,** 199-207.

GONZALEZ-CABRERA, P. J., BROWN, S., STUDER, S. M. & ROSEN, H. 2014. S1P signaling: new therapies and opportunities. *F1000Prime Rep,* 6**,** 109.

HOLLA, S., PRAKHAR, P., SINGH, V., KARNAM, A., MUKHERJEE, T., MAHADIK, K., PARIKH, P., SINGH, A., RAJMANI, R. S., RAMACHANDRA, S. G. & BALAJI, K. N. 2016. MUSASHI-Mediated Expression of JMJD3, a H3K27me3 Demethylase, Is Involved in Foamy Macrophage Generation during Mycobacterial Infection. *Plos Pathogens,* 12.

HOSONO, H., AOKI, J., NAGAI, Y., BANDOH, K., ISHIDA, M., TAGUCHI, R., ARAI, H. & INOUE, K. 2001. Phosphatidylserine-specific phospholipase A1 stimulates histamine release from rat peritoneal mast cells through production of 2-acyl-1-lysophosphatidylserine. *J Biol Chem,* 276**,** 29664-70.

IKUBO, M., INOUE, A., NAKAMURA, S., JUNG, S. J., SAYAMA, M., OTANI, Y., UWAMIZU, A., SUZUKI, K., KISHI, T., SHUTO, A., ISHIGURO, J., OKUDAIRA, M., KANO, K., MAKIDE, K., AOKI, J. & OHWADA, T. 2015. Structure-Activity Relationships of Lysophosphatidylserine Analogs as Agonists of G-Protein-Coupled Receptors GPR34, P2Y10, and GPR174. *Journal of Medicinal Chemistry,* 58**,** 4204-4219.

INOUE, A., ISHIGURO, J., KITAMURA, H., ARIMA, N., OKUTANI, M., SHUTO, A., HIGASHIYAMA, S., OHWADA, T., ARAI, H., MAKIDE, K. & AOKI, J. 2012. TGFalpha shedding assay: an accurate and versatile method for detecting GPCR activation. *Nat. Methods,* 9**,** 1021-9.

ISHII, I., FUKUSHIMA, N., YE, X. & CHUN, J. 2004. Lysophospholipid receptors: signaling and biology. *Annu Rev Biochem.,* 73**,** 321-54.

IWASHITA, M., MAKIDE, K., NONOMURA, T., MISUMI, Y., OTANI, Y., ISHIDA, M., TAGUCHI, R., TSUJIMOTO, M., AOKI, J., ARAI, H. & OHWADA, T. 2009a. Synthesis and evaluation of lysophosphatidylserine analogues as inducers of mast cell degranulation. Potent activities of lysophosphatidylthreonine and its 2-deoxy derivative. *Journal of Medicinal Chemistry,* 52**,** 5837-63.

IWASHITA, M., MAKIDE, K., NONOMURA, T., MISUMI, Y., OTANI, Y., ISHIDA, M., TAGUCHI, R., TSUJIMOTO, M., AOKI, J., ARAI, H. & OHWADA, T. 2009b. Synthesis and evaluation of lysophosphatidylserine analogues as inducers of mast cell degranulation. Potent activities of lysophosphatidylthreonine and its 2-deoxy derivative. *J Med Chem,* 52**,** 5837-63.

JOSHI, A., SHAIKH, M., SINGH, S., RAJENDRAN, A., MHETRE, A. & KAMAT, S. S. 2018. Biochemical characterization of the PHARC-associated serine hydrolase ABHD12 reveals its preference for very-long-chain lipids. *Journal of Biological Chemistry,* 293**,** 16953-16963.

KAMAT, S. S., CAMARA, K., PARSONS, W. H., CHEN, D. H., DIX, M. M., BIRD, T. D., HOWELL, A. R. & CRAVATT, B. F. 2015. Immunomodulatory lysophosphatidylserines are regulated by ABHD16A and ABHD12 interplay. *Nat Chem Biol,* 11**,** 164-71.

KELKAR, D. S., RAVIKUMAR, G., MEHENDALE, N., SINGH, S., JOSHI, A., SHARMA, A. K., MHETRE, A., RAJENDRAN, A., CHAKRAPANI, H. & KAMAT, S. S. 2019. A chemical-genetic screen identifies ABHD12 as an oxidized-phosphatidylserine lipase. *Nat Chem Biol,* 15**,** 169-178.

LEE, S. Y., LEE, H. Y., KIM, S. D., JO, S. H., SHIM, J. W., LEE, H. J., YUN, J. & BAE, Y. S. 2008. Lysophosphatidylserine stimulates chemotactic migration in U87 human glioma cells. *Biochem Biophys Res Commun,* 374**,** 147-51.

LIANG, Q. L., WU, Q. A., JIANG, J. H., DUAN, J. A., WANG, C., SMITH, M. D., LU, H., WANG, Q., NAGARKATTI, P. & FAN, D. P. 2011. Characterization of Sparstolonin B, a

Chinese Herb-derived Compound, as a Selective Toll-like Receptor Antagonist with Potent Anti-inflammatory Properties. *Journal of Biological Chemistry,* 286**,** 26470-26479.

LIANG, Q. L., YU, F., CUI, X. D., DUAN, J. A., WU, Q. N., NAGARKATTI, P. & FAN, D. P. 2013. Sparstolonin B suppresses lipopolysaccharide-induced inflammation in human umbilical vein endothelial cells. *Archives of Pharmacal Research,* 36**,** 890-896.

LLORET, S. & MORENO, J. J. 1995. Ca2+ influx, phosphoinositide hydrolysis, and histamine release induced by lysophosphatidylserine in mast cells. *J Cell Physiol.,* 165**,** 89-95.

MALLIK, S., PRASAD, R., BHATTACHARYA, A. & SEN, P. 2018. Synthesis of Phosphatidylserine and Its Stereoisomers: Their Role in Activation of Blood Coagulation. *Acs Medicinal Chemistry Letters,* 9**,** 434-439.

MEURER, S. K., NESS, M., WEISKIRCHEN, S., KIM, P., TAG, C. G., KAUFFMANN, M., HUBER, M. & WEISKIRCHEN, R. 2016. Isolation of Mature (Peritoneum-Derived) Mast Cells and Immature (Bone Marrow-Derived) Mast Cell Precursors from Mice. *Plos One,* 11.

NAPIER, C., MITCHELL, A. L., GAN, E., WILSON, I. & PEARCE, S. H. S. 2015. Role of the X-Linked Gene GPR174 in Autoimmune Addison's Disease. *Journal of Clinical Endocrinology & Metabolism,* 100**,** E187-E190.

NAPIER, C., MITCHELL, A. L., GAN, E. H., WILSON, I. & PEARCE, S. H. S. 2014. Female Proclivity to Autoimmune Addison's Disease: Role of the X-Linked Gene GPR174. *Endocrine Reviews,* 35.

OGASAWARA, D., ICHU, T. A., VARTABEDIAN, V. F., BENTHUYSEN, J., JING, H., REED, A., ULANOVSKAYA, O. A., HULCE, J. J., ROBERTS, A., BROWN, S., ROSEN, H., TEIJARO, J. R. & CRAVATT, B. F. 2018. Selective blockade of the lyso-PS lipase ABHD12 stimulates immune responses in vivo. *Nature Chemical Biology,* 14**,** 1099-1108.

PARK, K. S., LEE, H. Y., KIM, M. K., SHIN, E. H. & BAE, Y. S. 2005. Lysophosphatidylserine stimulates leukemic cells but not normal leukocytes. *Biochem Biophys Res Commun.,* 333**,** 353-358.

ROSEN, H., STEVENS, R. C., HANSON, M., ROBERTS, E. & OLDSTONE, M. B. 2013. Sphingosine-1-phosphate and its receptors: structure, signaling, and influence. *Annu Rev Biochem.,* 82**,** 637-62.

RUEDEN, C. T., SCHINDELIN, J., HINER, M. C., DEZONIA, B. E., WALTER, A. E., ARENA, E. T. & ELICEIRI, K. W. 2017. ImageJ2: ImageJ for the next generation of scientific image data. *BMC Bioinformatics,* 18**,** 529.

SHANBHAG, K., MHETRE, A., KHANDELWAL, N. & KAMAT, S. S. 2020. The Lysophosphatidylserines-An Emerging Class of Signalling Lysophospholipids. *J Membr Biol*.

SINGH, S., JOSHI, A. & KAMAT, S. S. 2020. Mapping the Neuroanatomy of ABHD16A, ABHD12, and Lysophosphatidylserines Provides New Insights into the Pathophysiology of the Human Neurological Disorder PHARC. *Biochemistry,* 59**,** 2299-2311.

SUGITA, K., YAMAMURA, C., TABATA, K. & FUJITA, N. 2013. Expression of orphan G-protein coupled receptor GPR174 in CHO cells induced morphological changes and proliferation delay via increasing intracellular cAMP. *Biochem Biophys Res Commun,* 430**,** 190-5.

SUGO, T., TACHIMOTO, H., CHIKATSU, T., MURAKAMI, Y., KIKUKAWA, Y., SATO, S., KIKUCHI, K., NAGI, T., HARADA, M., OGI, K., EBISAWA, M. & MORI, M. 2006. Identification of a lysophosphatidylserine receptor on mast cells. *Biochem Biophys Res Commun,* 341**,** 1078-87.

SZYMANSKI, K., MISKIEWICZ, P., PIRKO, K., JURECKA-LUBIENIECKA, B., KULA, D., HASSE-LAZAR, K., KRAJEWSKI, P., BEDNARCZUK, T. & PLOSKI, R. 2014. rs3827440, a nonsynonymous single nucleotide polymorphism within GPR174 gene in X chromosome, is associated with Graves' disease in Polish Caucasian population. *Tissue Antigens,* 83**,** 41-4.

TRACEY, T. J., STEYN, F. J., WOLVETANG, E. J. & NGO, S. T. 2018. Neuronal Lipid Metabolism: Multiple Pathways Driving Functional Outcomes in Health and Disease. *Frontiers in Molecular Neuroscience,* 11.

VAN DER KLEIJ, D., LATZ, E., BROUWERS, J. F., KRUIZE, Y. C., SCHMITZ, M., KURT-JONES, E. A., ESPEVIK, T., DE JONG, E. C., KAPSENBERG, M. L., GOLENBOCK, D. T., TIELENS, A. G. & YAZDANBAKHSH, M. 2002. A novel host-parasite lipid cross-talk. Schistosomal lyso-phosphatidylserine activates toll-like receptor 2 and affects immune polarization. *J Biol Chem.,* 277**,** 48122-9.

VANCE, J. E. 2015. Phospholipid Synthesis and Transport in Mammalian Cells. *Traffic,* 16**,** 1-18.

WU, C., JIN, X., TSUENG, G., AFRASIABI, C. & SU, A. I. 2016. BioGPS: building your own mash-up of gene annotations and expression profiles. *Nucleic Acids Res,* 44**,** D313-6.

WYMANN, M. P. & SCHNEITER, R. 2008. Lipid signalling in disease. *Nature Reviews Molecular Cell Biology,* 9**,** 162-176.
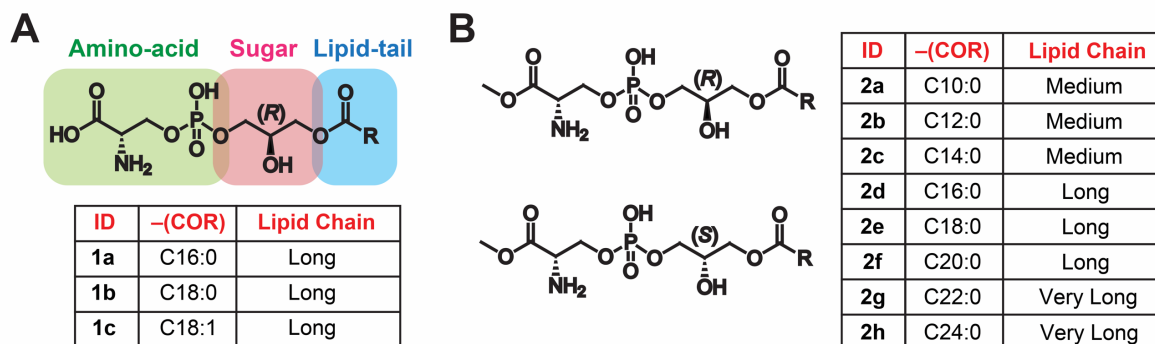
Figures and Figure Legends.

Figure 1. Lyso-PSs and Me-lyso-PSs. The chemical structures of (**A**) commercially available canonical natural lyso-PSs and (**B**) our synthetic Me-lyso-PS lipid library with both (*R*)- and (*S*)-stereoisomers.
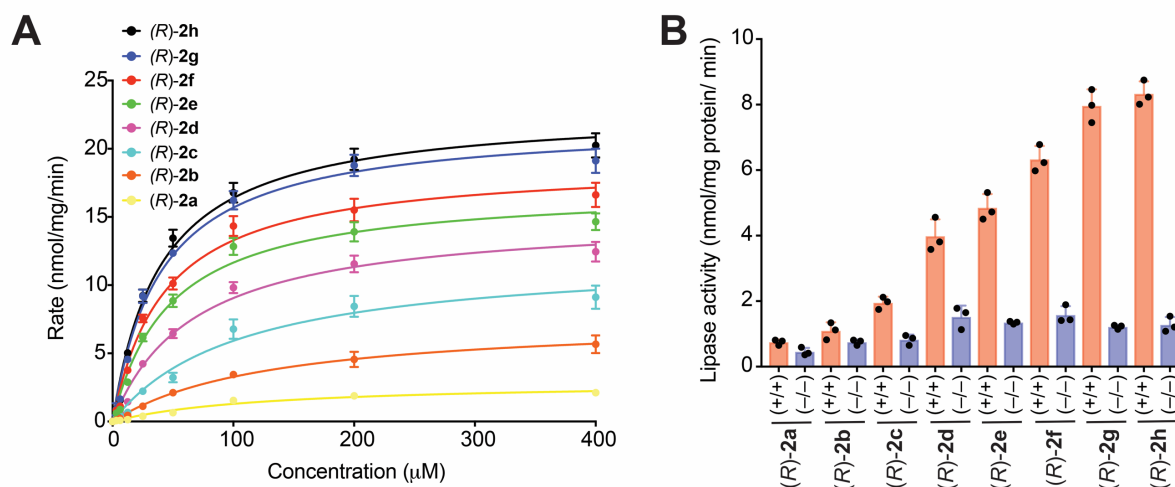

Figure 2. ABHD12 prefers VLC lyso-PSs as substrates. (**A**) Enzyme kinetic assays for membrane lysates (10 μg) of HEK293T cells transfected with hABHD12 tested against the (*R*)-Me-lyso-PSs (0 – 400 μM, 30 mins, 37 °C, n = 3/data point). The line connecting the points, represents a fit to the Michaelis-Menten enzyme kinetics equation. See **Table 1** for all enzyme kinetic parameters. (**B**) Lipid hydrolysis assays for (*R*)-Me-lyso-PSs (100 μM, 30 mins, 37 °C, n = 3/group) tested against brain membrane lysates (20 μg) from wild type (+/+) or ABHD12 knockout (–/–) mice. All data presented in (**A**, data points), and (**B**, bars) is represented as mean ± standard deviation.
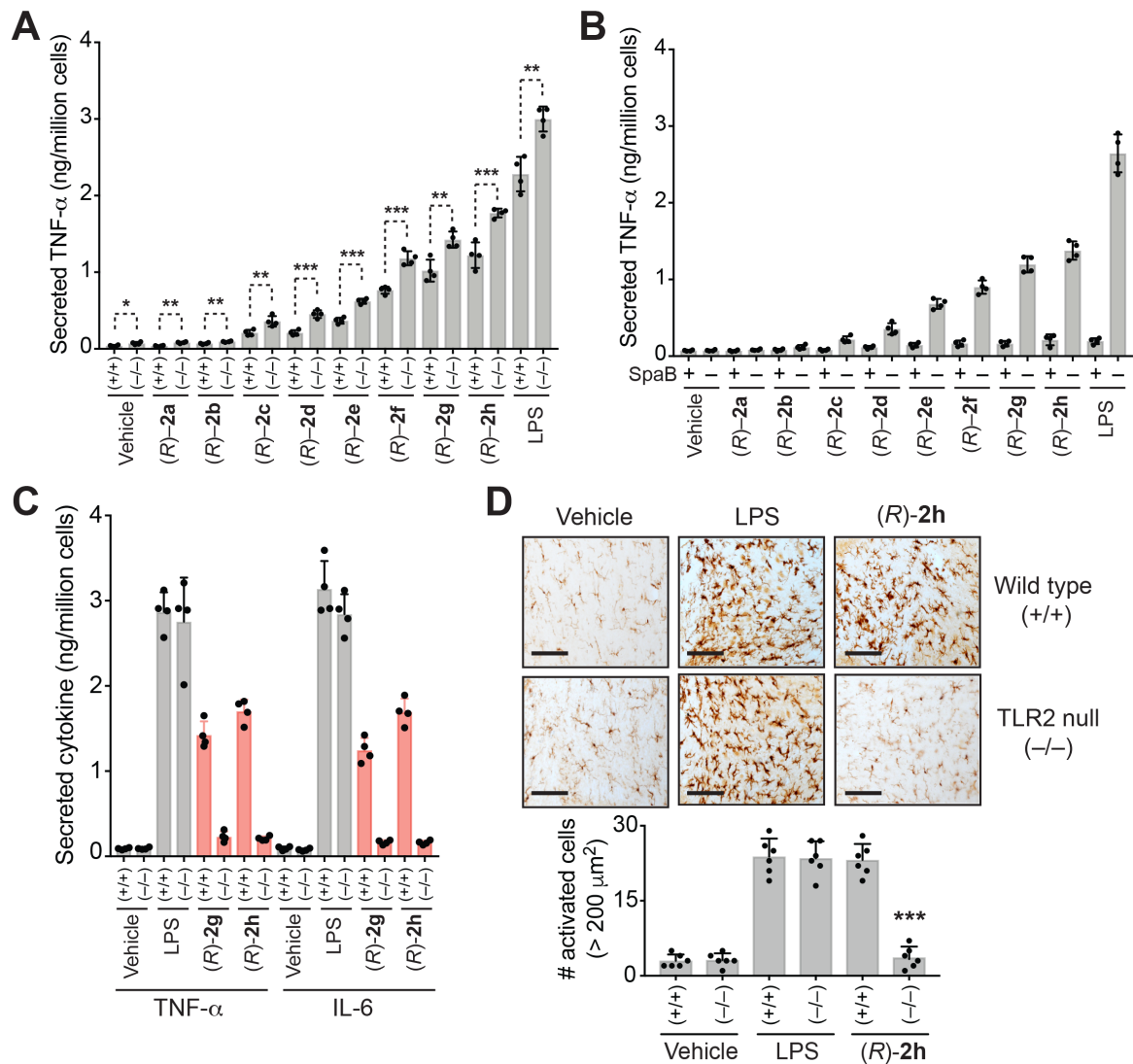
Figure 3. VLC lyso-PSs elicit pro-inflammatory responses via a TLR2 dependent pathway. Secreted TNF-α from PPM harvested from (**A**) wild type (+/+) or ABHD12 knockout (–/–) mice following treatment with vehicle (DMSO) or lipopolysaccharide (LPS) or (*R*)-**2a-h** (1 μM, 4 h, 37 $^{\circ}$C); (**B**) wild type mice pre-treated with DMSO or SpaB (10 μM, 4 h, 37 $^{\circ}$C), followed by treatment with vehicle or LPS or (*R*)-**2a-h** (1 μM, 4 h, 37 $^{\circ}$C); (**C**) wild type (+/+) or TLR2 knockout (–/–) mice following treatment with vehicle or LPS or VLC (*R*)-Me-lyso-PSs (1 μM, 4 h, 37 $^{\circ}$C, red bars highlight responses to VLC (*R*)-Me-lyso-PSs). (**D**) Representative images from Iba-1 immunostaining for microglial activation (black bar = 250 μm) and quantification of enlarged cells (>200 μm^2) in the cerebellum (per 1.44 mm^2) of wild type (+/+) or TLR2 knockout (–/–) mice following intravenous injection of vehicle (PBS), LPS or (*R*)-**2h** (all 1 mg/kg body weight, 10 h). All data presented in (**A**), (**B**), (**C**), and (**D**) is represented as mean $\pm$ standard deviation (n = 4-6/group). *$p < 0.05$, **$p < 0.01$, and ***$p < 0.001$ versus (+/+) group by Student's two-tailed t-test.
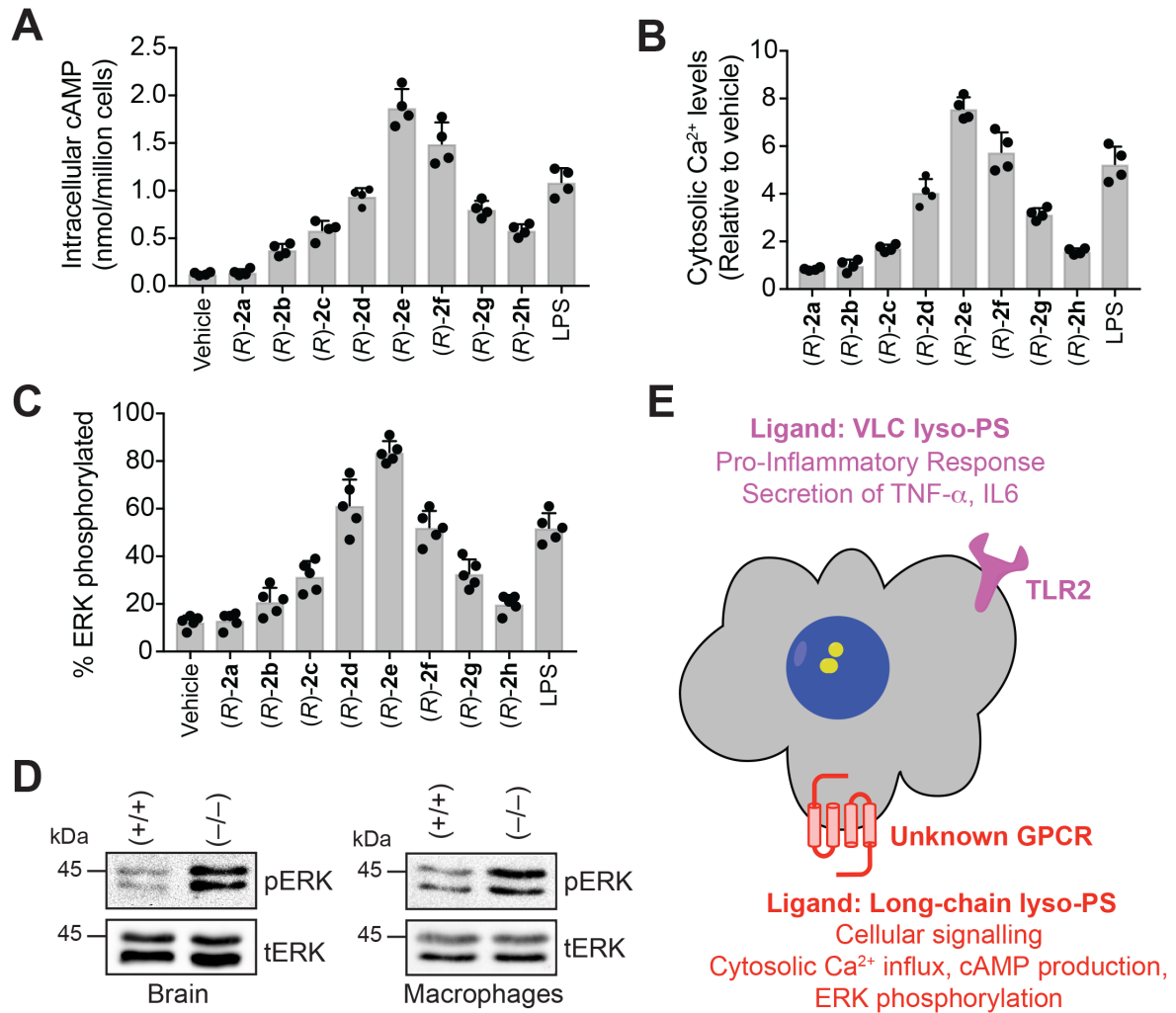
Figure 4. LC lyso-PSs activate macrophages through a GPCR. (**A**) Intracellular cAMP, (**B**) relative cytosolic Ca^{2+} levels, and (**C**) percentage of phosphorylated ERK from WT PPM following treatment with vehicle (DMSO) or LPS or (*R*)-**2a-h** (1 μM, 10 mins, 37 ^{o}C). All data presented in (**A**), (**B**), and (**C**) is represented as mean $\pm$ standard deviation (n = 5/group). (**D**) Representative western blots on lysates of brain (6-month-old mice) and LPS-treated (1 μM, 4 h, 37 ^{o}C) PPM harvested from wild type (+/+) or ABHD12 knockout (–/–) mice, showing enhanced ERK phosphorylation in both tissues for the (–/–) genotype. (**E**) Schematic cartoon representation of lyso-PS signaling pathways by two types of receptors in mammalian macrophages.
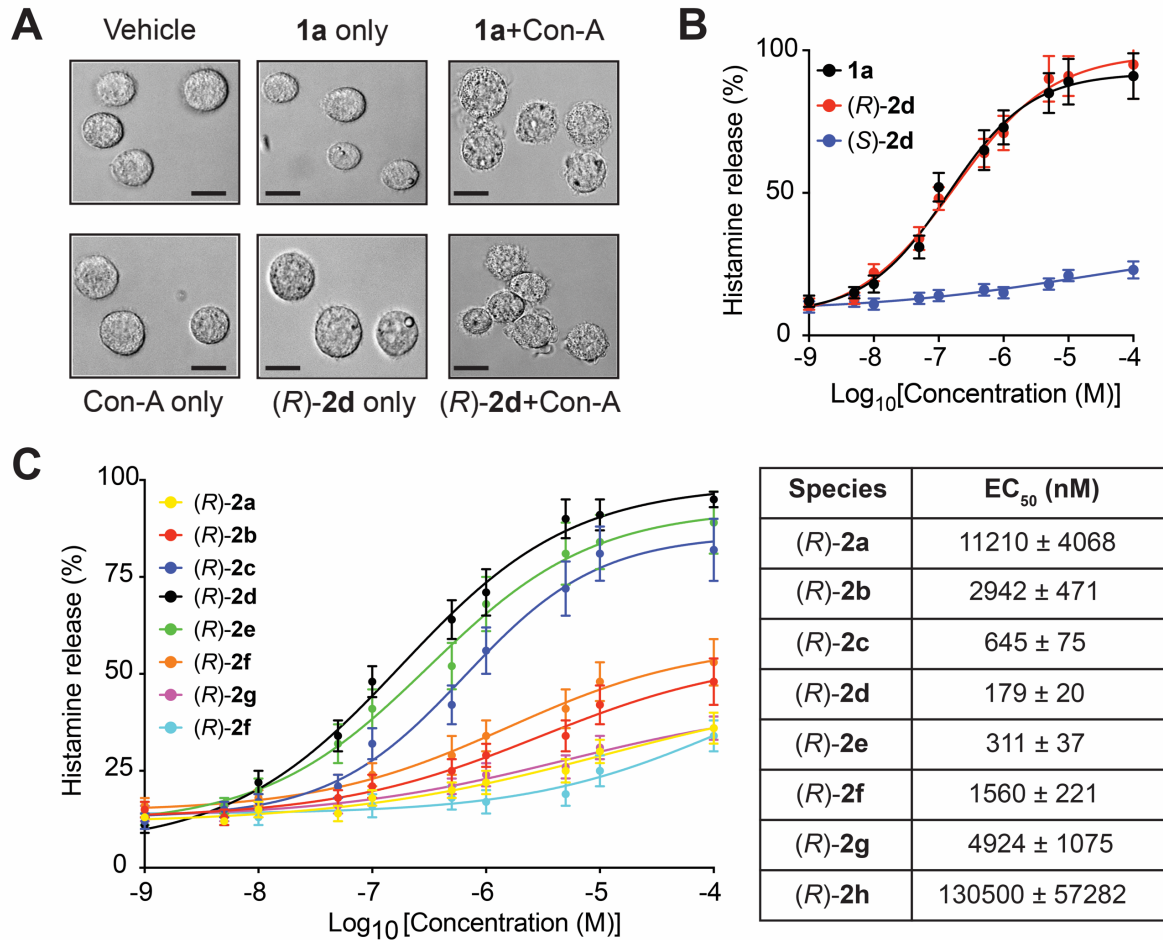
Figure 5. LC lyso-PSs robustly cause histamine release from primary mast cells. (**A**) Representative microscopy image showing degranulation of PCMCs after **1a** or (*R*)-**2d** treatment (both 1 μM, 30 mins, 37 ^{o}C) in the presence of concanavalin A (Con-A) (black bar = 100 μm). (**B**) Histamine release profile from PCMCs treated with **1a** or (*R*)-**2d** or (*S*)-**2d** (1 nM to 10 mM, 30 mins, 37 ^{o}C, n = 3/data point). (**C**) Dose response and EC_{50} values for histamine release from PCMCs following treatment with the different (*R*)-Me-lyso-PSs (1 nM to 10 mM, 30 mins, 37 ^{o}C, n = 3/data point).
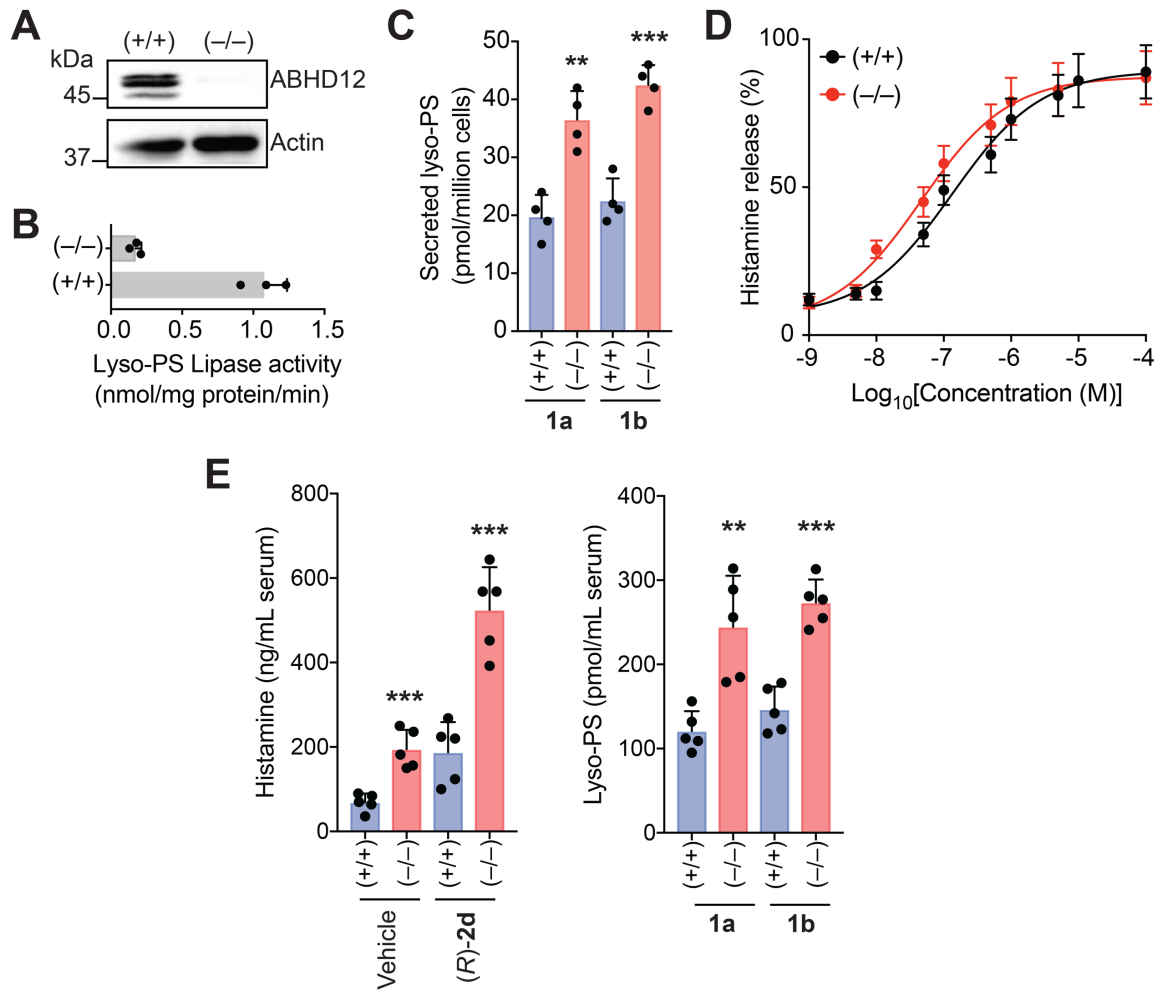
Figure 6. ABHD12 controls concentrations of LC lyso-PSs in mast cells, and thereby serum histamine levels. (**A**) Representative western blot and (**B**) lyso-PS lipase activity assay (100 μM **1a**, 30 mins, 37 °C, n = 3/group), showing the loss of ABHD12 in PCMCs derived from ABHD12 knockout (–/–) mice. (**C**) Concentrations of lyso-PS secreted from cultured PCMCs derived from wild type (+/+) or ABHD12 knockout (–/–) mice, showing significantly increased **1a** and **1b** secretion from ABHD12-null PCMCs (n = 4/group). (**D**) Histamine release profiles from PCMCs derived from wild type (+/+) or ABHD12 knockout (–/–) mice treated with **1a** (1 nM to 10 mM, 30 mins, 37 °C, n = 3/data point). (**E**) *Left*, Serum histamine levels in (+/+) or (–/–) mice following intravenous injections with vehicle (PBS) or (*R*)-**2d** (1 mg/kg, 2 h), showing increased serum histamine concentrations in the (–/–) mice compared to (+/+) controls for both treatments (n =5/group). Interestingly, systemic administration of (*R*)-**2d** in (+/+) mice, produces significantly more circulating serum histamine compared to the vehicle group, showing that (*R*)-**2d** by itself can induce histamine release from mast cells in *in vivo* settings. *Right*, Serum lyso-PS concentrations in (+/+) or (–/–) mice, showing increased concentrations of circulating **1a** and **1b** in (–/–) mice, corroborating the increased serum histamine levels seen in these mice (n = 5/group). All data presented in this figure is represented as mean ± standard deviation from at least n independent experiments. **$p < 0.01$, and ***$p < 0.001$ versus (+/+) group by Student's two-tailed t-test.

Table 1: Kinetic constants for lyso-PS and Me-lyso-PS substrates tested against recombinantly expressed hABHD12 (HEK293T membrane lysates transiently transfected with hABHD12).

Lyso-PS species	Fatty acid chain length: unsaturation	V_{max} (nmol/mg protein/min)	K_M (μM)	V_{max}/K_M (nmol/mg protein/min/M) (x 10^5)
1a	16:0	15.6 ± 0.6	72 ± 8	2.2 ± 0.3
1b	18:0	18.3 ± 0.5	48 ± 4	3.8 ± 0.4
1c	18:1	17.8 ± 0.6	46 ± 6	3.8 ± 0.5
(*R*)-**2a**	10:0	2.9 ± 0.2	126 ± 18	0.2 ± 0.04
(*R*)-**2b**	12:0	7.6 ± 0.3	131 ± 14	0.6 ± 0.06
(*R*)-**2c**	14:0	12.2 ± 0.6	106 ± 14	1.1 ± 0.1
(*R*)-**2d**	16:0	15.2 ± 0.6	67 ± 7	2.3 ± 0.3
(*R*)-**2e**	18:0	17.2 ± 0.6	47 ± 5	3.7 ± 0.5
(*R*)-**2f**	20:0	19.0 ± 0.6	43 ± 4	4.4 ± 0.5
(*R*)-**2g**	22:0	22.0 ± 0.6	40 ± 4	5.5 ± 0.6
(*R*)-**2h**	24:0	22.9 ± 0.6	40 ± 4	5.7 ± 0.6
(*S*)-**2a**	10:0	0.2 ± 0.02	275 ± 32	0.007 ± 0.001
(*S*)-**2b**	12:0	0.4 ± 0.05	255 ± 35	0.016 ± 0.002
(*S*)-**2c**	14:0	0.6 ± 0.1	215 ± 28	0.028 ± 0.003
(*S*)-**2d**	16:0	0.8 ± 0.1	187 ± 24	0.043 ± 0.006
(*S*)-**2e**	18:0	1.2 ± 0.1	178 ± 25	0.067 ± 0.008
(*S*)-**2f**	20:0	1.3 ± 0.2	165 ± 23	0.078 ± 0.009
(*S*)-**2g**	22:0	1.2 ± 0.2	167 ± 26	0.072 ± 0.009
(*S*)-**2h**	24:0	1.2 ± 0.3	176 ± 31	0.068 ± 0.008